Research Square

Preprints are preliminary reports that have not undergone peer review.
They should not be considered conclusive, used to inform clinical practice,
or referenced by the media as validated information.

ZnO and Ni-doped ZnO photocatalysts: Synthesis, characterization and improved visible light driven photocatalytic degradation of methylene blue

Iqbal Ahmad
Xian Jiaotong University: Xi'an Jiaotong University
Mehwish Aslam
Allama Iqbal Open University
Uzma Jabeen
Sardar Bahadur Khan Women's University
Muhammad Nadeem Zafar (znadeempk@gmail.com)
University of Gujrat https://orcid.org/0000-0002-2109-7601
Muhammad Najam Khan Malghani
BUITEMS: Balochistan University of Information Technology and Management Sciences
Norah Alwadai
Princess Nourah bint Abdulrahman University
Fwzah H. Alshammari
University of Hafr Al Batin
Amani Saleh Almuslem
King Faisal University
Zahid Ullah
Allama Iqbal Open University

Research Article

Keywords: ZnO, Photocatalytic degradation, Band gap tuning, Ni doping, Photocatalyst

Posted Date: May 10th, 2022

DOI: https://doi.org/10.21203/rs.3.rs-1576671/v1

License: This work is licensed under a Creative Commons Attribution 4.0 International License.
Read Full License

Abstract

The nickel modified zinc oxide (ZnO) photocatalysts with nominal composition of $Zn_{1-x}Ni_xO$ (x = 0.0–0.5) were synthesized by wet chemical approach. Optical studies were performed using Fourier transformed infrared (FTIR), electronic spectroscopy and X-ray diffraction (XRD) methods. Scanning electron microscopy (SEM) complimented with Energy Dispersive X-ray (EDX) was used to study the morphology and chemical composition of prepared photocatalysts. A significant hypsochromic shift has been observed with respect to un-doped ZnO nanocatalyst due to quantum confinement effect. Subsequently, the band gap has been tuned to the region of lower wavelength. X-ray results reveal that ZnO nanocatalyst are in hexagonal crystalline form. In addition, the effect of nickel impurity on photocatalytic activity of ZnO nanocatalysts in degradation of methylene blue (MB) was also investigated. Degradation results showed that the MB was degraded more effectively by Ni-doped ZnO photocatalysts due to large band gap under visible light irradiation.

Highlights

- ZnO and Ni-doped ZnO nanocatalysts have been synthesized by wet chemical method.
- UV-Visible absorption spectra witness bathochromic shift due to quantum confinement effect.
- XRD results reveal that nanocatalysts exist in hexagonal crystalline state.
- Degradation results shows that the MB is degraded more effectively by Ni-doped ZnO.
- Ni doping results in large band gap decreased recombination process.

Introduction

Nanotechnology is an appealing field among various branches of science. Amazing properties are associated with the small size of nanomaterials (Heiligtag and Niederberger 2013). The foremost purpose of nanoscience is to tune and limit the material size at nanoscale (1-100 nm) to form devices with excellent performances (Hsu et al. 2018). Nanomaterials are used in variety of fields like fuel cells, solar cells, super capacitors, biosensors, resonant devices, adsorption, and catalysis (Kallem et al. 2019; Khan et al. 2019; Wang and Wolfbeis 2020; Wickramasinghe et al. 2019). Synthesis of metal oxides especially transition metal oxides nanoparticles is the main focus of researchers working in the field of nanotechnology (Choi et al. 2019) and as semiconductors, these materials play an important role in electronics, catalysis, solar energy conversion and storage devices (Bibi et al. 2019; Lin et al. 2019; Zhao et al. 2018). Semiconductor adsorbents have shown their capability to detoxify the organic pollutants (Zafar et al. 2018).

One of the important water pollutants is dye stuff released form industries (Liu et al. 2019b). For the industrial effluent treatment, the semiconductors (TiO_2, ZnO etc.) as photocatalysts are used to degrade the dye stuff present in the industrial wastewater (Scarisoreanu et al. 2017; Song et al. 2018). Photocatalytic degradation by semiconductor materials is an effective, unique, and fast approach (Liu et

al. 2019a; Xie and Li 2006). Although, TiO_2 is an effective catalyst for degradation of dyes under visible light irradiation but its high cost is the major barrier towards its application on commercial scale. Therefore, for the industrial effluent treatment, it is highly desirable to find the economical semiconductor photocatalysts which possess reasonable energy band gap, improved adsorption properties, effective degradation properties, and better visible light harvesting properties (Diebold 2003; Stylidi et al. 2003).

ZnO is a low-cost semiconductor with reasonable band gap (3.2 eV). It demonstrates remarkable properties, which are due to its unique physical and chemical properties *viz.* high electrochemical coupling, stability, and excellent light harvesting capacity (Kuriakose et al. 2014) and in photocatalysis, it can be used as superlative alternative of TiO_2. Photocatalytic activity of ZnO is highly affected due to photo induced electron hole pair aggregation phenomenon. However, its visible light harvesting response is very poor and possibility of photo-corrosion is also very high. To address these issues, nano-junction system of multiple constituents (Au, Ag, Si) or doping (Cd, Al, Cu) strategies have been employed by many researcher (Ahmad et al. 2016a; Javed Iqbal et al. 2012). Light harvesting properties can also be tuned by metal accumulation on the surface of ZnO or addition of metal ion impurity or preparing composite of ZnO with other semiconducting material (Lahiri and Batzill 2008; Zhang et al. 2004).

Herein, we report different Ni-doped ZnO nanocrystals as photocatalysts. For this purpose, a series of Ni-doped ZnO nanocatalysts with altering Ni impurity has been prepared and their photocatalytic activities have been assessed employing methylene blue (MB) as a model organic pollutant. Moreover, UV-Visible spectra of pure and Ni-doped ZnO photocatalysts have been recorded and band gap energies have been calculated from their spectra employing Tauc equation. The effect of Ni contents on band gap energies of ZnO and its resultant effect on photocatalytic activity have been studied in detail.

Experimental

Chemicals

Zinc nitrate, nickel nitrate and ammonia solution were obtained from Sigma Aldrich and used for synthesis of nanocatalysts. Doubly distilled water and methanol were used as medium for synthesis. MB was also obtained from Sigma Aldrich.

Synthesis of ZnO and Ni-doped ZnO nanocatalysts

ZnO nanocatalysts have been synthesized using wet chemical approach. To synthesize ZnO nanocatalysts, 50 mL of 0.1 M $Zn(NO_3)_2$ solution was prepared in distilled water and stirred at 25°C. After that, 28% aqueous ammonia solution was added drop wise into $Zn(NO_3)_2$ solution to obtain the pH of about 8. At this pH, white precipitate was appeared, and solution was further stirred for 40 min. Next, the precipitate was cleaned with doubly distilled water and ethyl alcohol several times and then dried in oven at 120°C for 1 h. After that, nanocatalysts were annealed at 380°C in furnace for 40 min (Singh et al. 2012).

For Ni-doped ZnO nanocatalysts synthesis, 0.1 M $Zn(NO_3)_2$ and 0.1 M $Ni(NO_3)_2$ solutions were prepared separately. For $Zn_{0.96}Ni_{0.04}O$ nanoparticles, 2 mL $Ni(NO_3)_2$ solution was added into 48 mL of $Zn(NO_3)_2$ solution and kept in reaction vessel with continues stirring. Next, 28% aqueous ammonia was added in a $Ni(NO_3)_2$ /$Zn(NO_3)_2$ solution to attain pH of 8. After the formation of white precipitates, the stirring process was continued for 30 min. Subsequently, precipitates were washed by doubly distilled water and ethanol for multiple times. Next, precipitates were dried in oven at 120°C for 1 h. After that, nanocatalysts were annealed at 380°C in furnace for 40 min (Singh et al. 2012). Similar procedure has been adopted for the synthesis of other Ni-doped ZnO nanocatalysts by adding the stoichiometric amounts of Zn^{2+} and Ni^{2+} from their precursor salts solutions.

Characterization of ZnO and Ni-doped ZnO nanocatalysts

To evaluate the optical properties of ZnO and Ni-doped ZnO nanocatalysts. the Fluorescence (PL) spectrophotometer (Perkin Elmer, model LS 55) and UV-Visible spectrophotometer (Shimadzu 1601) were used. Fourier Transformed Infra-Red spectrometer (Nicolet 6700 in the ATR mode) was employed for FTIR studies. To explore crystallinity and purity of nanomaterials, X-ray Diffraction (XRD) was used. Chemical composition was determined by Energy Dispersive X-ray (EDX) and size and morphology of synthesized nanocatalysts were investigated using Scanning Electron Microscope (SEM) (MIRA3 TESCAN).

Photocatalytic degradation activity of ZnO and Ni-doped ZnO nanocatalysts

To study the photocatalytic degradation of MB, an amount of 10 mg of photocatalyst (ZnO, Ni-doped ZnO) was dispersed in 50 mL of 3 ppm aqueous MB solution. Then, reaction mixture was stirred for 60 min at room temperature under dark conditions to attain adsorption-desorption equilibrium between photocatalyst and MB. After that, reaction mixture was placed under visible light irradiation. 2 mL of MB solution was withdrawn after every 10 min to observe the degradation process by taking absorption spectra using UV-Visible spectrophotometer. The optical density of MB before and after irradiation at regular intervals of time has been used to calculate the percentage degradation efficiency (%D) of photocatalysts using the following Eq. 1 (Jabeen et al. 2017):

$$\%D = \frac{A_o - A_t}{A_o} \times 100 \quad 1$$

Where A_o and A_t are absorbance recoded initially and absorbance recorded at different times respectively. The mechanism of photocatalytic degradation of MB using ZnO and Ni-doped ZnO photocatalysts is presented in Scheme 1a, b, respectively.

Results And Discussion

Characterization of ZnO and Ni-doped ZnO nanocatalysts

X-ray diffractograms of pure and Ni-doped ZnO nanocatalysts are displayed in Fig. 1. From the Fig. 1, it is observed that, seven prominent diffraction peaks are observed at angles (2θ) of 31.1°, 33.9°, 35.6°, 47.0°, 56.1°, 62.4°, and 67.6° for planes (100), (002), (101), (102), (110), (103) and (112) respectively in un-doped and Ni-doped ZnO nanocatalysts, which depict the formation of hexagonal wurtzite crystalline form and is in accordance with the JCPDS card number 36-1451. Further, it is clear from the X-ray diffractograms, Ni-doped ZnO nanocatalysts demonstrate exactly similar diffraction patterns, which may be the clear evidence of successful incorporation of Ni in ZnO lattice. Additionally, a slight shift in diffraction peaks of Ni-doped ZnO samples than the pure ZnO has been observed. According to Vegard's law, dopant ion does not exhibit diffraction peak, but it is responsible in the shift of diffraction peaks of host material. It is further noted that the peak height of diffraction peaks declines significantly with the increment of Ni content, indicating that the crystalline nature of ZnO diminishes with Ni impurity. Furthermore, the ionic radius of Zn^{2+} and Ni^{2+} are 74 and 69 pm, respectively. Doping with a light atom can expect a smaller intensity and doping with a heavy atom produce opposite result. Additionally, the broadened peaks in X-ray diffractograms of ZnO and Ni-doped ZnO might be the indication of smaller particles. The decrease in particle size and increase in band gap due to increment of Ni impurity into ZnO lattice is also evident from UV-Visible spectra of photocatalysts. The crystallite size has been calculated by employing following Debye-Sherrer equation (Ahmad et al. 2016b):

$$\mathrm{D} = \frac{0.89\lambda}{\beta\cos\theta} \quad 2$$

Where D, β and λ are crystallite size, peak width and wavelength of x-rays used to record X-ray diffractograms, respectively. The crystallite sizes of pure and Ni-doped ZnO nanocatalysts have been determined from more intense 101 peak for all the samples and their values are given in Table 1.

Table 1
Crystallite size and optical band gap of ZnO and Ni-doped ZnO nanocatalysts

Sample composition	Crystallite size (nm)	Optical band gap (ev)	Increment in band gap (ev)	Decrease in band gap (ev)
ZnO	10.0	2.56	-	-
$Zn_{0.96}Ni_{0.04}O$	12.5	2.33	-	0.23
$Zn_{0.90}Ni_{0.10}O$	11.0	3.62	0.06	-
$Zn_{0.88}Ni_{0.12}O$	9.00	3.66	0.10	-
$Zn_{0.86}Ni_{0.14}O$	11.5	2.50	-	0.06

The size and morphology of photocatalysts plays an important role in photocatalytic activity. SEM micrographs were captured to investigate the surface morphology of the pure and Ni-doped ZnO nanocatalysts. SEM micrographs of ZnO, $Zn_{0.96}Ni_{0.04}O$ and $Zn_{0.88}Ni_{0.12}O$ photocatalysts are displayed in Fig. 2. SEM micrographs indicate that all nanocatalysts are sphere-shaped and even in size and have clear boundary. Additionally, it is obvious from the SEM micrographs that for all the samples, particles are agglomerated. An average particle size of 55, 48 and 41 nm for ZnO, $Zn_{0.96}Ni_{0.04}O$ and $Zn_{0.88}Ni_{0.12}O$ respectively has been calculated from SEM micrographs and it suggests that increasing Ni contents, particle size decreases, which complements UV-Visible results. The elemental composition of pure and Ni-doped ZnO nanocatalysts has been examined by EDX analysis. The EDX spectrum of ZnO (Fig. 2) indicates the predominance of zinc and oxygen with their composition (weight%) 79.35% and 20.65% respectively. Where Fig. 2(b) is the EDX spectrum of Ni-doped ZnO ($Zn_{0.96}Ni_{0.04}O$) nanocatalyst and it reveals the peaks of zinc, oxygen, and nickel with their composition (weight%) 77.82%, 21.99% and 0.19% respectively. Similarly, EDX spectrum of Ni-doped ZnO ($Zn_{0.88}Ni_{0.12}O$) nanocatalyst presented in Fig. 2(c) shows the peaks of zinc, oxygen and nickel with their composition (weight%) 66.85%, 32.12% and 1.03% respectively, which verifies an effective doping of Ni metal ion in ZnO lattice. The mass percent and atomic percent data for pure and Ni-doped ZnO nanocatalysts are presented in Table 2.

Table 2
Chemical composition of ZnO, $Zn_{0.96}Ni_{0.04}O$ and $Zn_{0.88}Ni_{0.12}O$

Sample	Weight %			Atomic %		
	Zn	O	Ni	Zn	O	Ni
ZnO	79.35	20.65	0	48.46	51.54	0
$Zn_{0.96}Ni_{0.04}O$	77.82	21.99	0.19	46.35	53.52	0.13
$Zn_{0.88}Ni_{0.12}O$	66.85	32.12	1.03	33.56	65.87	0.57

Fourier transformed infrared spectroscopy (FTIR) is an excellent tool for the confirmation of presence of metal oxygen bonds in oxides of different metals. FTIR spectra of synthesized pure and Ni-doped ZnO nanocatalysts are exhibited in Fig. 3. The peak noted at 1557.93 cm^{-1} is attributed to the bond between zinc and oxygen (Dandeneau et al. 2009) and the absorption peak at 3389.57 cm^{-1} is associated with OH^- for water, which is due to the adsorbed moisture in the samples. The peak observed at about 1512.48 cm^{-1} indicates the existence of NO_3^- ion, which has not been removed from samples during washing. The two broad absorption bands observed at 3389.57 cm^{-1} and 1048.69 cm^{-1} are due to the NH_2 and N-H groups, respectively. In the FTIR spectra of Ni-doped ZnO nanocatalysts, the absorption band observed in the range of 3283.81 to 3390.51 cm^{-1} is ascribed to Ni-ZnO bond (Dandeneau et al.

2009; Vafaee and Ghamsari 2007) and presence of this peak indicates successful incorporation of Ni metal in ZnO lattice.

UV-Visible spectroscopic results of pure and Ni-doped ZnO nanocatalysts are shown in Fig. 4. The un-doped ZnO nanocatalyst exhibits the absorption band at 370 nm. Figure 4 also demonstrates the absorption bands for different concentrations of Ni impurity in ZnO lattice. The content of Ni impurity in substituted ZnO varies from 2 to 14%. The band positions show hypsochromic (blue shift) with boosting the concentration of Ni. The absorption band is witnessed at 379 nm for 2% Ni impurity in ZnO. In addition, there is a constant tuning of absorption band to the lower wavelength with increasing Ni content in ZnO lattice resulting in increased band gap, which in turn results in the decrease of particle size. Consequently, there is small opportunity of the recombination of electron from conduction band (CB) to valence band (VB). Kubelka-Munk (KM) model has been employed to calculate the values of energy band gap (E_g) of photocatalysts by plotting $(ahυ)^{1/2}$ against $hυ$ (Tauc plot) (Su et al. 2017). Table 1 shows increase and decrease in band gap values with respect to un-doped sample with Ni contents. Figure 5 displays Tauc plots of pure and Ni-doped ZnO nanocatalysts. Furthermore, the change in the band gap of doped sample with respect to un-doped ZnO, is an obvious indication for the replacement of Ni in ZnO crystal structure. The tuning of band gap might be attributed to the exchange interactions of electrons present in sp and d orbitals of the divalent nickel ions. The performance of photocatalysts in terms of their photocatalytic activity can also be explained by the magnitudes of work function of Ni and Zn which is ~ 5.15 eV and ~ 4.33 eV respectively as it restricts the promotion of electrons from lower work function Zn to higher work function Ni by forming a Schottky barrier (Drummond 1999). Under light irradiation, the holes are generated due to the migration of electrons from VB to CB. This photo-excitation results in the transfer of electrons from Zn to Ni due to the higher work function and interacts with oxygen which in turn generates reactive oxidative species involved in dye degradation reaction.

Photoluminescence (PL) spectroscopy is an appropriate method to study the distribution of energy among the released photons that are resulted from photo-excitation process in a specific wavelength range, which can help to examine the role of electron-hole pair in polycrystalline semiconductors. It is useful technique to study the charge transfer process, distortion in lattice and calculation of oxygen vacancies within the system. Figure 6 shows PL spectra recorded at room temperature for pure and Ni-doped ZnO nanocatalysts at excitation wavelength of 370 nm. Two emission peaks are observed, first peak at 398 nm in ultraviolet region attributable to the band gap excitonic emission and second at 776 nm in visible region ascribed to the oxygen vacancies, which is resulted from deficiency of oxygen in ZnO lattice (Huang et al. 2001; Williams and Kamat 2009). Further, it has also been observed from PL spectra of Ni-doped ZnO nanocatalysts that with enhancing the content of Ni impurity, a blue shift is observed in the visible region and can be justified in the light of defects, which are produced by introducing impurity in the lattice of ZnO. Additionally, it was noticed that the PL intensity decreases with increasing the concentration of Ni impurity in ZnO lattice. By enhancing the Ni impurity in ZnO, the probability of recombination of electrons and holes in the valence band has decreased, which results in a small decrease in the PL intensity in Ni-doped ZnO sample than that of un-doped ZnO sample.

Photocatalytic degradation of MB using ZnO and Ni-doped ZnO photocatalysts

To investigate the visible light assisted photocatalytic activity of the pure and Ni-doped ZnO nanocatalysts, MB has been subjected to degradation with these photocatalysts. To eliminate the adsorption factor by photocatalysts from the results, adsorption-desorption equilibrium has been achieved by overnight stirring of MB solution with photocatalyst under dark conditions and for further studies this adsorption-desorption equilibrium has been selected as initial concentration of MB.

The photocatalytic performance of pure and Ni-doped ZnO photocatalysts for MB degradation has been studied by employing the UV-Visible spectrometer and the obtained spectra of MB with different photocatalysts under visible light irradiation are presented in Fig. 7. It has been noticed for each photocatalyst that with irradiation time, optical density of the band perceived at 664 nm of MB substantially decreases and during the complete course of reaction, no additional peak has been found. It is clear from the obtained results, ZnO photocatalyst degrades MB with slower rate, while Ni-doped ZnO photocatalysts demonstrate enhanced performance due to Ni doping. Doping enhances the photocatalytic activity because it reduces the recombination chance of electrons and holes due to greater charge separation in Ni doped samples. Furthermore, Ni substitution trap electrons and reduce the possibility of charge recombination, which is the major cause of inhibition of the photocatalytic process (Sanchez and Lopez 1995). Additionally, the concentration of OH^- radicals and oxygen species is also increased, which also results in increased performance of Ni-doped ZnO photocatalysts (Kato et al. 2005). Apart from all these factors, as discussed earlier, work function of Ni and Zn metals also plays a significant part in the enhanced photocatalytic activity of Ni-doped ZnO photocatalysts. This observation can also be supported by the fact that properties of semiconductors can significantly be altered by doping of other metal ions, operating conditions and synthesis method (Lee et al. 2016).

The percentage degradation efficiency against the irradiation time and time resolved concentration profiles (C/C_o *vs.* time plots) of pure and Ni-doped ZnO photocatalysts are presented in Figs. 8 and 9, respectively. It can be observed that maximum MB degradation is obtained by $Zn_{0.88}Ni_{0.12}O$ photocatalyst, when compared to pure and other Ni-doped ZnO ($Zn_{0.96}Ni_{0.04}O$, $Zn_{0.90}Ni_{0.10}O$ and $Zn_{0.86}Ni_{0.14}O$) photocatalysts. The different performance exhibited by photocatalysts is due to band gap of pure and metal substituted nanomaterial. With increase in band gap, particle size decreases and consequently, possibility of recombination of electron-hole is reduced. Under visible light irradiation, the photocatalytic efficiency is also boosted by oxygen vacancies (Cao et al. 2013). The percentage degradation efficiencies of pure and Ni-doped ZnO photocatalysts are summarized in Table 3. To evaluate the reusability and stability of the catalysts, they were collected from the reaction mixture and were used again. All the catalysts demonstrate reproducible efficiency. The maximum loss (%) in degradation efficiency has been observed to be ~ 3% for ZnO and minimum for Ni-doped ZnO (Table 3). These results indicate that Ni doping reduces the photocorrosion of ZnO which in turn enhances its stability.

Table 3
Photodegradation efficiency, rate constant (*k*) and loss in activity after first use for MB degradation employing ZnO and Ni-doped ZnO photocatalysts

Sr. No.	Time (min)	% degradation efficiency				
		ZnO	$Zn_{0.96}Ni_{0.04}O$	$Zn_{0.90}Ni_{0.10}O$	$Zn_{0.88}Ni_{0.12}O$	$Zn_{0.86}Ni_{0.14}O$
1	0	0	0	0	0	0
2	10	30	35	38	50	35
3	20	42	64	66	75	41
4	30	69	72	82	83	63
5	40	78	85	86	87	68
6	50	80	89	92	95	85
7	60	93	92	95	98	89
k ($\times 10^{-2}$ min^{-1})		4.8	4.0	4.6	8.1	2.8
% loss in activity after first use		3.3	2.6	2.4	2.1	2.1

The photocatalytic degradation reaction of MB follows pseudo-first first order kinetics and the integrated rate equation used for this process is (Cui et al. 2016):

$$ln\frac{C}{C_0} = k\mathrm{t} \quad 3$$

Where C_o and C are concentrations of MB at the beginning and at time t., while k is pseudo-first order rate constant. The plots of $ln(C/C_o)$ *vs.* time for MB degradation process using un-doped and Ni-doped ZnO photocatalysts are displayed in Fig. 10. It is clear from these plots that in each case data is well fitted and obey the Eq. (3). The values of pseudo-first order rate constant are given in Table 3. The maximum value (8.1 $x10^{-2}$ min^{-1}) of k has been observed for $Zn_{0.88}Ni_{0.12}O$ and minimum (2.8 $x10^{-2}$ min^{-1}) for $Zn_{0.86}Ni_{0.14}O$ (8.1 $x10^{-2}$ min^{-1}) photocatalyst and is in accordance with the percentage degradation results.

Conclusions

Un-doped and Ni-doped ZnO photocatalysts have been effectively prepared by wet chemical approach at room temperature. The synthesized nanomaterials were confirmed by XRD, FTIR, SEM, EDX, and UV-Visible spectroscopy. The absorption band is shifted towards the lower wavelength with increment of Ni impurity and results in decrease in particle size. X-ray diffractogram revealed that the ZnO nanocatalysts

possess wurtzite hexagonal structure. SEM micrographs exhibited that synthesized samples have ordered shape and uniform size. In XRD patterns, no additional peak of nickel impurity has been witnessed which confirms the efficacious substitution of metal in ZnO structure. $Zn_{0.88}Ni_{0.12}O$ photocatalyst exhibited the maximum efficiency with higher rate for the degradation of MB. This improved photocatalytic degradation efficiency of $Zn_{0.88}Ni_{0.12}O$ due to Ni substitution in ZnO is related with the band gap tuning.

Declarations

Author contributions

Iqbal Ahmad: Funding acquisition, supervision, conceptualization, writing – review & editing. **Mehwish Aslam**: Writing – original draft, methodology, investigation. **Uzma Jabeen**: Writing – review & editing, investigation. **Muhammad Nadeem Zafar**: Supervision, conceptualization, writing - review & editing. **Muhammad Najam Khan Malghani**: Writing – review & editing, methodology. **Norah Alwadai**: Writing – review & editing. **Fwzah H. Alshammari**: Funding acquisition, writing – review & editing. **Amani Saleh Almuslem**: Writing – review & editing. **Zahidullah**: Writing – review & editing, validation.

Declaration of competing interest

The authors declare that they have no known and unknown competing financial interests that could influence the work reported in this paper.

Acknowledgements

The authors are greatly thankful to Higher Education Commission of Pakistan for PC1 project, and Allama Iqbal Open University, Islamabad, Pakistan for providing space and laboratory facilities. The authors also acknowledge the financial support through NRPU project (6515/Punjab/NRPU/R&D/HEC/2016) awarded by Higher Education Commission of Pakistan.

References

1. Ahmad I, Shah SM, Ashiq MN, Khan RA (2016a) Effect of Nd3+ and Cd2+ ions co-substitution on the dielectric and electron transport properties of spinel strontium nanoferrites Ceramics International 42:12763-12770
2. Ahmad I et al. (2016b) Fabrication of Nd^{3+} and Mn^{2+} ions Co-doped Spinal Strontium Nanoferrites for High Frequency Device Applications Journal of Electronic Materials 45:4979-4988 doi:10.1007/s11664-016-4653-8
3. Bibi N et al. (2019) Mesoporous Ce2Zr2O7/PbS nanocomposite with an excellent supercapacitor electrode performance and cyclic stability ChemistrySelect 4:655-661

4. Cao Y, Yu Y, Zhang P, Zhang L, He T, Cao Y (2013) An enhanced visible-light photocatalytic activity of TiO2 by nitrogen and nickel–chlorine modification Separation and Purification Technology 104:256-262
5. Choi D et al. (2019) Quantum scale biomimicry of low dimensional growth: An unusual complex amorphous precursor route to TiO2 band confinement by shape adaptive biopolymer-like flexibility for energy applications Scientific Reports 9:18721 doi:10.1038/s41598-019-55103-z
6. Cui X, Xu W, Xie Z, Dorman JA, Gutierrez-Wing MT, Wang Y (2016) Effect of dopant concentration on visible light driven photocatalytic activity of Sn 1− x Ag x S 2 Dalton Transactions 45:16290-16297
7. Dandeneau CS, Jeon Y-H, Shelton CT, Plant TK, Cann DP, Gibbons BJ (2009) Thin film chemical sensors based on p-CuO/n-ZnO heterocontacts Thin Solid Films 517:4448-4454
8. Diebold U (2003) The surface science of titanium dioxide Surface science reports 48:53-229
9. Drummond TJ (1999) Work functions of the transition metals and metal silicides. Sandia National Labs., Albuquerque, NM (US), Sandia National Labs …,
10. Heiligtag FJ, Niederberger M (2013) The fascinating world of nanoparticle research Materials Today 16:262-271
11. Hsu S-W, Rodarte AL, Som M, Arya G, Tao AR (2018) Colloidal Plasmonic Nanocomposites: From Fabrication to Optical Function Chem Rev 118:3100-3120 doi:10.1021/acs.chemrev.7b00364
12. Huang MH, Wu Y, Feick H, Tran N, Weber E, Yang P (2001) Catalytic growth of zinc oxide nanowires by vapor transport Advanced materials 13:113-116
13. Jabeen U, Shah SM, Khan SU (2017) Photo catalytic degradation of Alizarin red S using ZnS and cadmium doped ZnS nanoparticles under unfiltered sunlight Surfaces and Interfaces 6:40-49
14. Javed Iqbal M, Ahmad Z, Meydan T, Melikhov Y (2012) Physical, electrical and magnetic properties of nano-sized Co-Cr substituted magnesium ferrites Journal of applied physics 111:033906
15. Kallem P, Yanar N, Choi H (2019) Nanofiber-Based Proton Exchange Membranes: Development of Aligned Electrospun Nanofibers for Polymer Electrolyte Fuel Cell Applications ACS Sustainable Chemistry & Engineering 7:1808-1825 doi:10.1021/acssuschemeng.8b03601
16. Kato S, Hirano Y, Iwata M, Sano T, Takeuchi K, Matsuzawa S (2005) Photocatalytic degradation of gaseous sulfur compounds by silver-deposited titanium dioxide Applied Catalysis B: Environmental 57:109-115
17. Khan NA, Rashid N, Junaid M, Zafar MN, Faheem M, Ahmad I (2019) NiO/NiS heterostructures: an efficient and stable electrocatalyst for oxygen evolution reaction ACS Applied Energy Materials 2:3587-3594
18. Kuriakose S, Satpati B, Mohapatra S (2014) Enhanced photocatalytic activity of Co doped ZnO nanodisks and nanorods prepared by a facile wet chemical method Physical Chemistry Chemical Physics 16:12741-12749
19. Lahiri J, Batzill M (2008) Surface functionalization of ZnO photocatalysts with monolayer ZnS The Journal of Physical Chemistry C 112:4304-4307

20. Lee KM, Lai CW, Ngai KS, Juan JC (2016) Recent developments of zinc oxide based photocatalyst in water treatment technology: a review Water research 88:428-448
21. Lin X et al. (2019) Rational synthesis of CaCo2O4 nanoplate as an earth-abundant electrocatalyst for oxygen evolution reaction Journal of energy chemistry 31:125-131
22. Liu J et al. (2019a) F/W co-doped TiO2-SiO2 composite aerogels with improved visible light-driven photocatalytic activity Journal of Solid State Chemistry 275:8-15
23. Liu L, Mu B, Li W, Yang Y (2019b) Semistable emulsion system based on spent cooking oil for pilot-scale reactive dyeing with minimal discharges ACS Sustainable Chemistry & Engineering 7:13698-13707
24. Sanchez E, Lopez T (1995) Effect of the preparation method on the band gap of titania and platinum-titania sol-gel materials Materials Letters 25:271-275
25. Scarisoreanu M et al. (2017) High photoactive TiO2/SnO2 nanocomposites prepared by laser pyrolysis Appl Surf Sci 418:491-498 doi:https://doi.org/10.1016/j.apsusc.2016.12.122
26. Singh O, Singh MP, Kohli N, Singh RC (2012) Effect of pH on the morphology and gas sensing properties of ZnO nanostructures Sensors and Actuators B: Chemical 166:438-443
27. Song L, Wang Y, Ma J, Zhang Q, Shen Z (2018) Core/shell structured Zn/ZnO nanoparticles synthesized by gaseous laser ablation with enhanced photocatalysis efficiency Applied Surface Science 442:101-105
28. Stylidi M, Kondarides DI, Verykios XE (2003) Pathways of solar light-induced photocatalytic degradation of azo dyes in aqueous TiO2 suspensions Applied Catalysis B: Environmental 40:271-286
29. Su Y et al. (2017) A layered wide-gap oxyhalide semiconductor with an infinite ZnO 2 square planar sheet: Sr 2 ZnO 2 Cl 2 Chemical Communications 53:3826-3829
30. Vafaee M, Ghamsari MS (2007) Preparation and characterization of ZnO nanoparticles by a novel sol–gel route Materials Letters 61:3265-3268
31. Wang X-d, Wolfbeis OS (2020) Fiber-Optic Chemical Sensors and Biosensors (2015–2019) Anal Chem 92:397-430 doi:10.1021/acs.analchem.9b04708
32. Wickramasinghe D, Oh J-M, McGraw S, Senecal K, Chow K-F (2019) Electrochemical Effects of Depositing Iridium Oxide Nanoparticles onto Conductive Woven and Nonwoven Flexible Substrates ACS Applied Energy Materials 2:372-381 doi:10.1021/acsaem.8b01404
33. Williams G, Kamat PV (2009) Graphene– semiconductor nanocomposites: excited-state interactions between ZnO nanoparticles and graphene oxide Langmuir 25:13869-13873
34. Xie YB, Li XZ (2006) Interactive oxidation of photoelectrocatalysis and electro-Fenton for azo dye degradation using TiO2–Ti mesh and reticulated vitreous carbon electrodes Mater Chem Phys 95:39-50 doi:https://doi.org/10.1016/j.matchemphys.2005.05.048
35. Zafar MN, Amjad M, Tabassum M, Ahmad I, Zubair M (2018) SrFe2O4 nanoferrites and SrFe2O4/ground eggshell nanocomposites: fast and efficient adsorbents for dyes removal Journal

of Cleaner Production 199:983-994

36. Zhang M, An T, Hu X, Wang C, Sheng G, Fu J (2004) Preparation and photocatalytic properties of a nanometer ZnO–SnO2 coupled oxide Applied Catalysis A: General 260:215-222
37. Zhao D et al. (2018) Efficient two-terminal all-perovskite tandem solar cells enabled by high-quality low-bandgap absorber layers Nature Energy 3:1093-1100 doi:10.1038/s41560-018-0278-x

Scheme

Scheme 1 is available in Supplementary Files section.

Figures

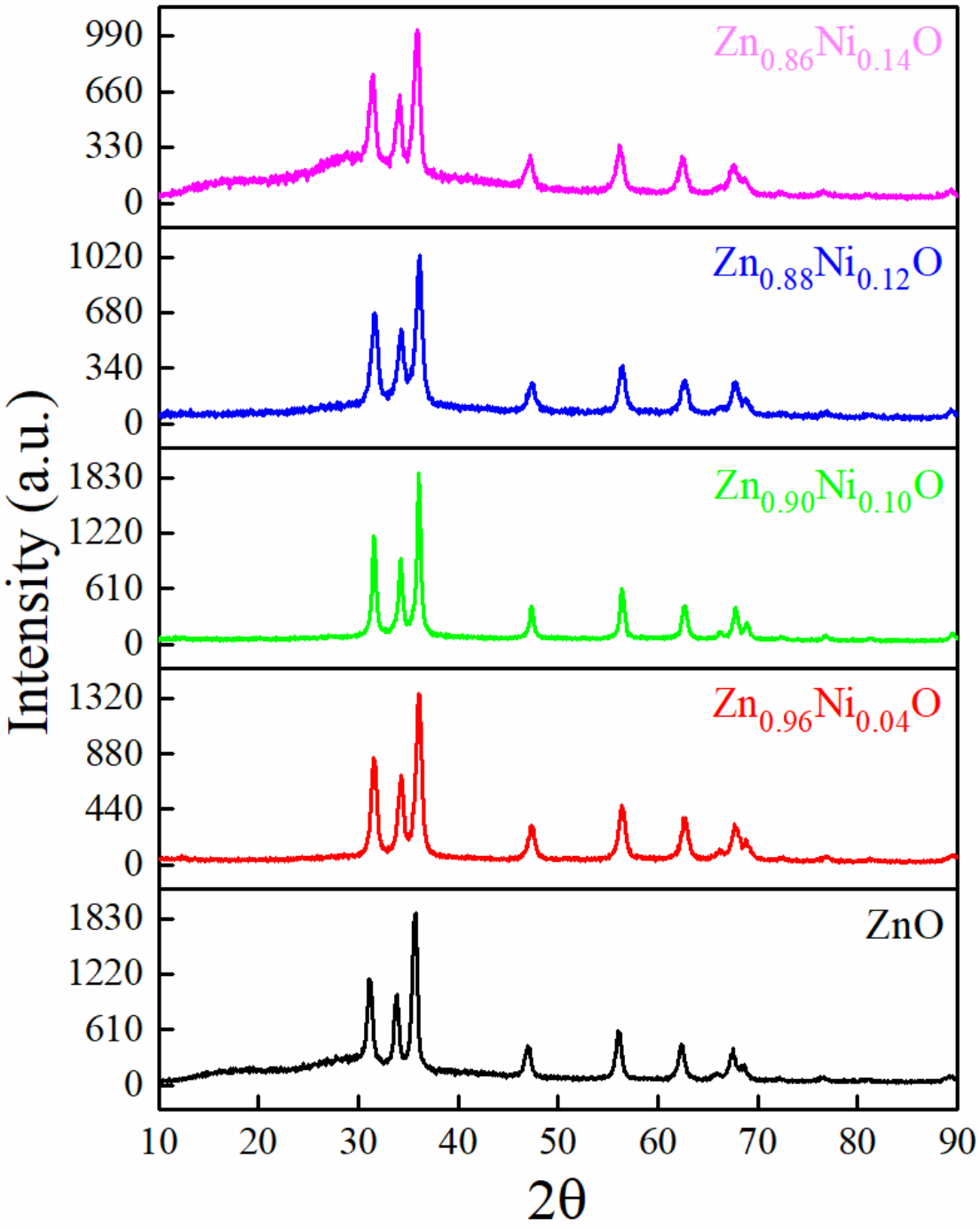

Figure 1

XRD spectra of ZnO (black), $Zn_{0.96}Ni_{0.04}O$ (red), $Zn_{0.9}Ni_{0.1}O$ (green), $Zn_{0.88}Ni_{0.12}O$ (blue) and $Zn_{0.86}Ni_{0.14}O$ (magenta) nanocatalysts.

Figure 2

SEM images and EDS spectrum of (a) ZnO, (b) $Zn_{0.96}Ni_{0.04}O$ and (c) $Zn_{0.88}Ni_{0.12}O$ nanocatalysts.

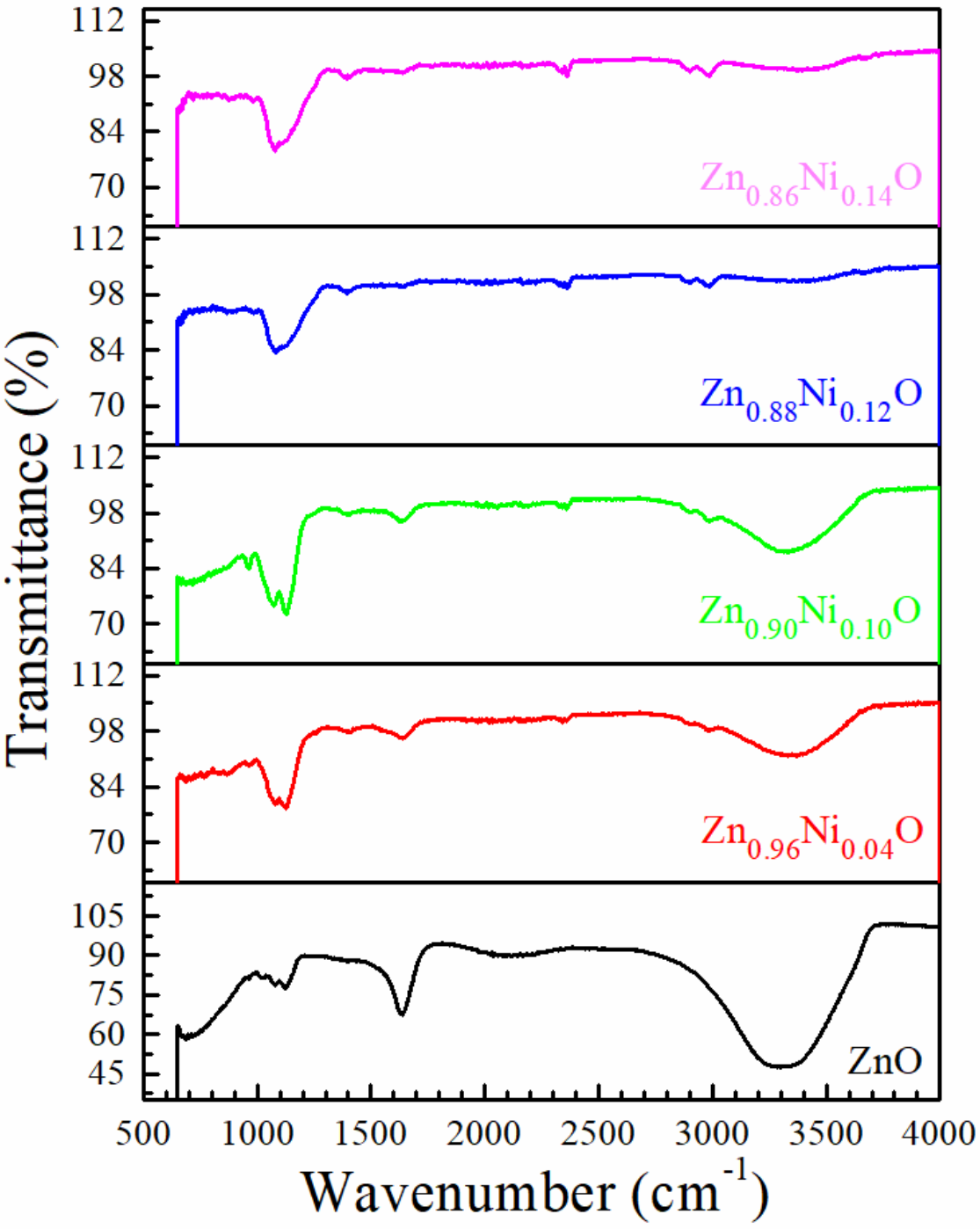

Figure 3

FTIR spectra of ZnO (black), $Zn_{0.96}Ni_{0.04}O$ (red), $Zn_{0.90}Ni_{0.10}O$ (green), $Zn_{0.88}Ni_{0.12}O$ (blue) and $Zn_{0.86}Ni_{0.14}O$ (magenta) nanocatalysts.

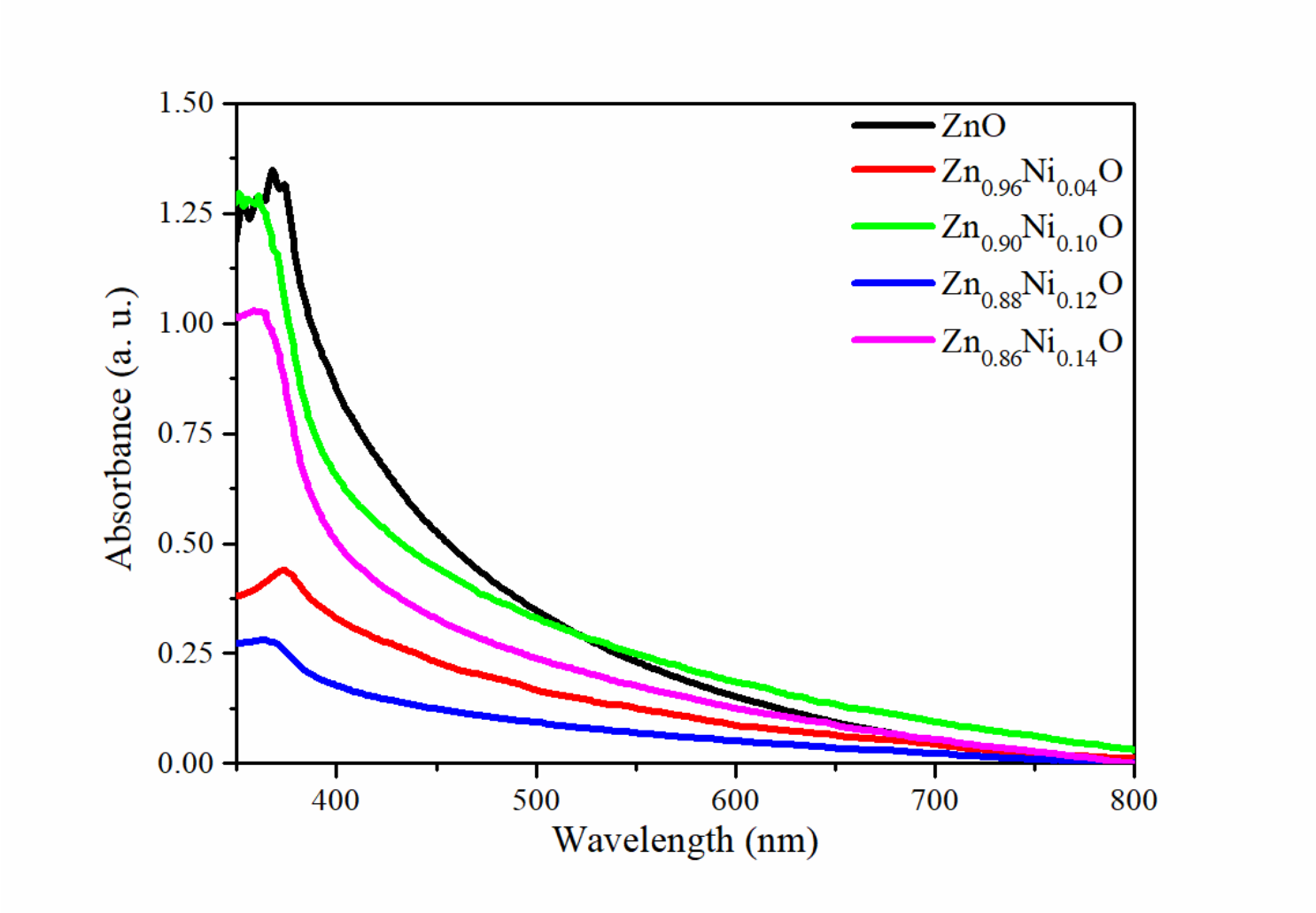

Figure 4

Electronic spectra of ZnO (black), $Zn_{0.96}Ni_{0.04}O$ (red), $Zn_{0.90}Ni_{0.10}O$ (green), $Zn_{0.88}Ni_{0.12}O$ (blue) and $Zn_{0.86}Ni_{0.14}O$ (magenta) nanocatalysts

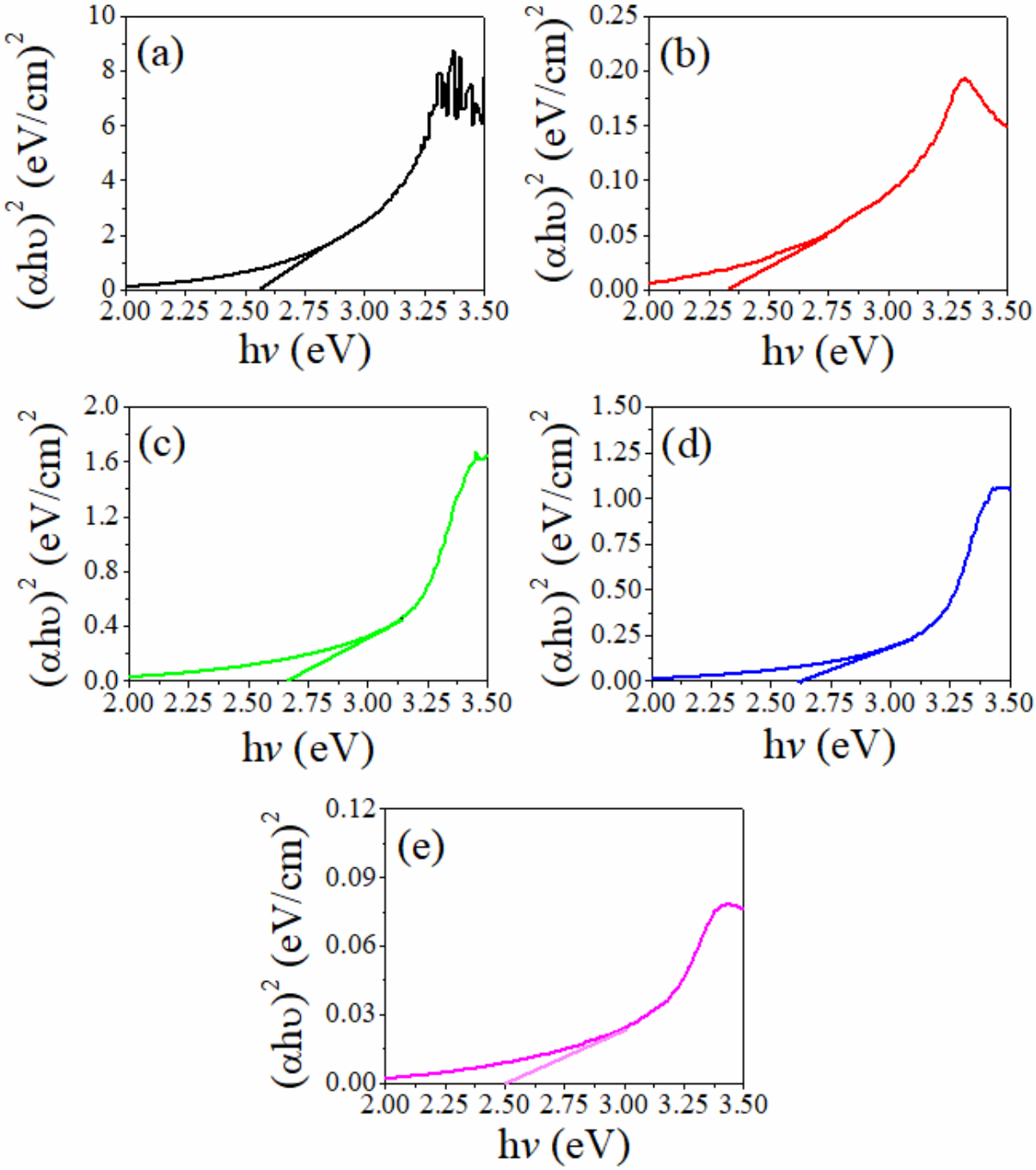

Figure 5

Tauc plots of (a) ZnO, (b) $Zn_{0.96}Ni_{0.04}O$, (c) $Zn_{0.90}Ni_{0.10}O$, (d) $Zn_{0.88}Ni_{0.12}O$ and (e) $Zn_{0.86}Ni_{0.14}O$ nanocatalysts.

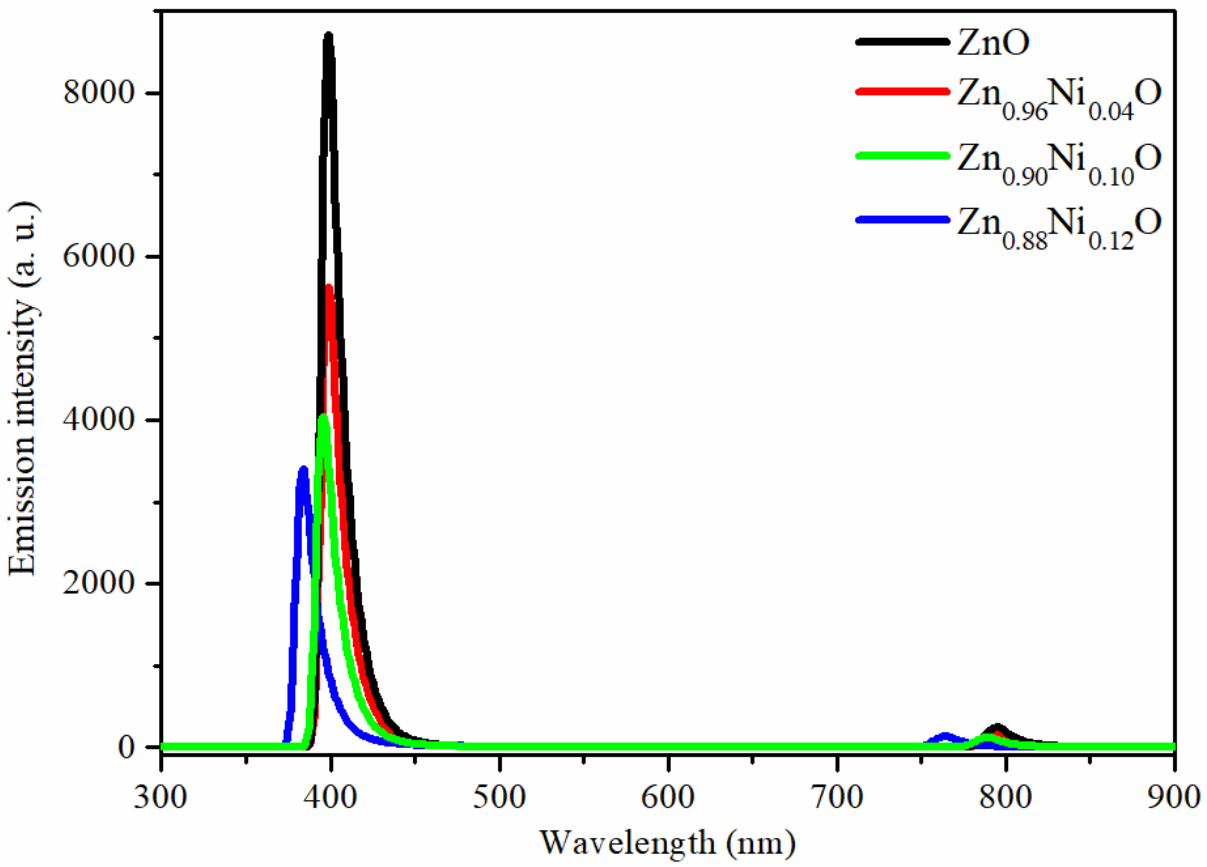

Figure 6

PL spectra of ZnO (black), $Zn_{0.96}Ni_{0.04}O$ (red), $Zn_{0.90}Ni_{0.10}O$ (green) and $Zn_{0.88}Ni_{0.12}O$ (blue) nanocatalysts.

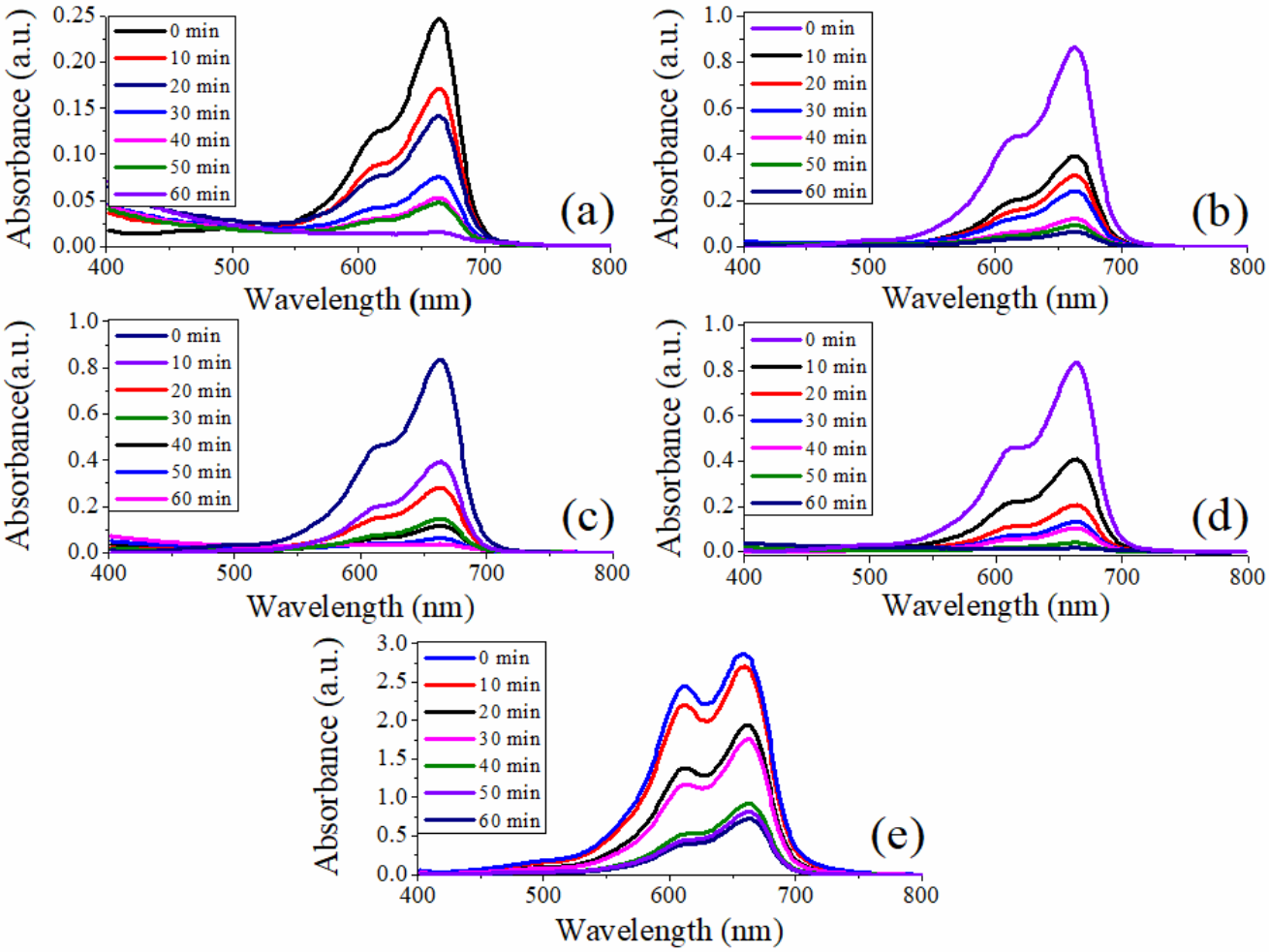

Figure 7

UV-Visible spectra for degradation of MB onto (a) ZnO, (b) $Zn_{0.96}Ni_{0.04}O$, (c) $Zn_{0.90}Ni_{0.10}O$, (d) $Zn_{0.88}Ni_{0.12}O$ and (e) $Zn_{0.86}Ni_{0.14}O$ photocatalysts.

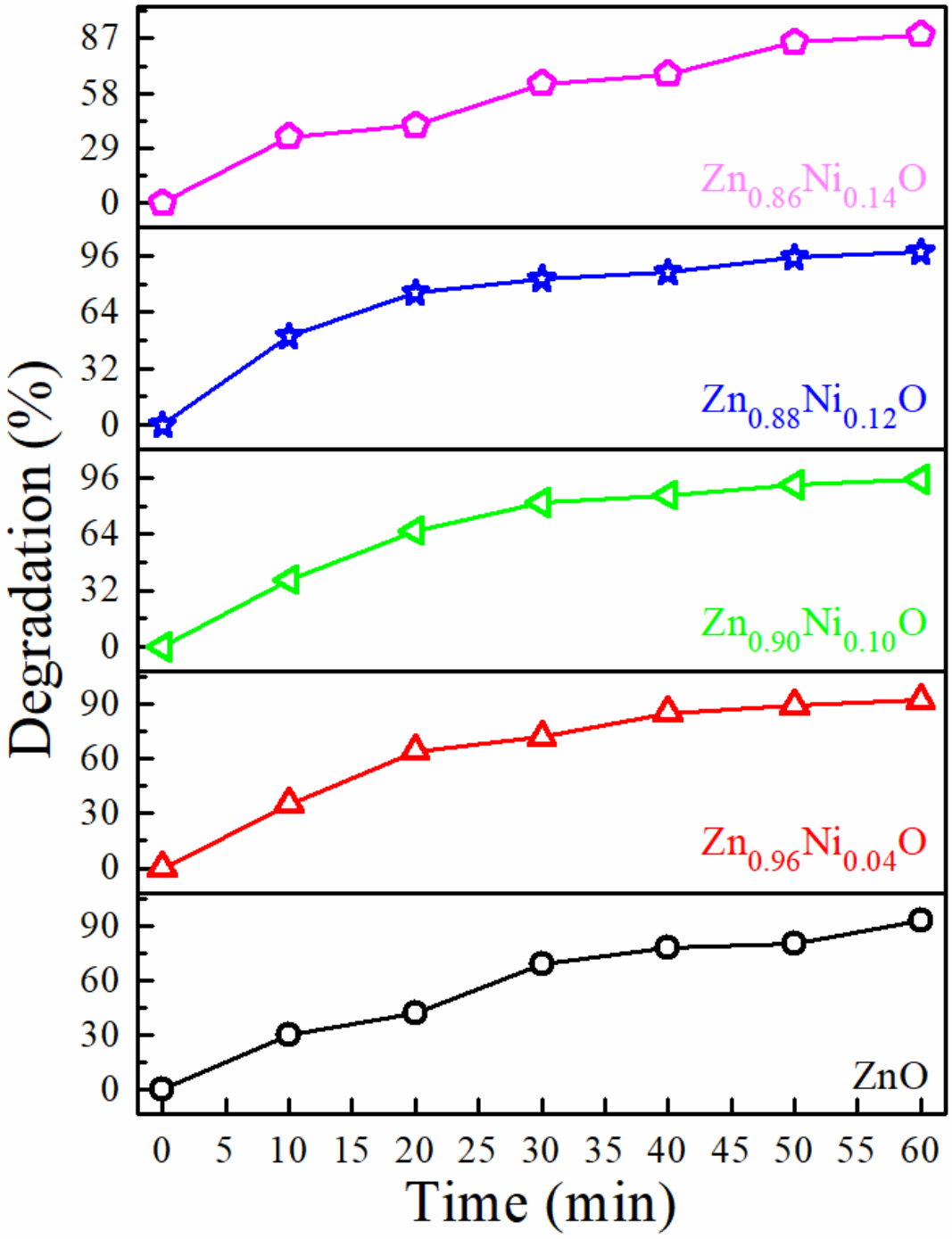

Figure 8

Degradation efficiency of MB onto ZnO (black), $Zn_{0.96}Ni_{0.04}O$ (red), $Zn_{0.90}Ni_{0.10}O$ (green), $Zn_{0.88}Ni_{0.12}O$ (blue) and $Zn_{0.86}Ni_{0.14}O$ (magenta) nano photocatalysts.

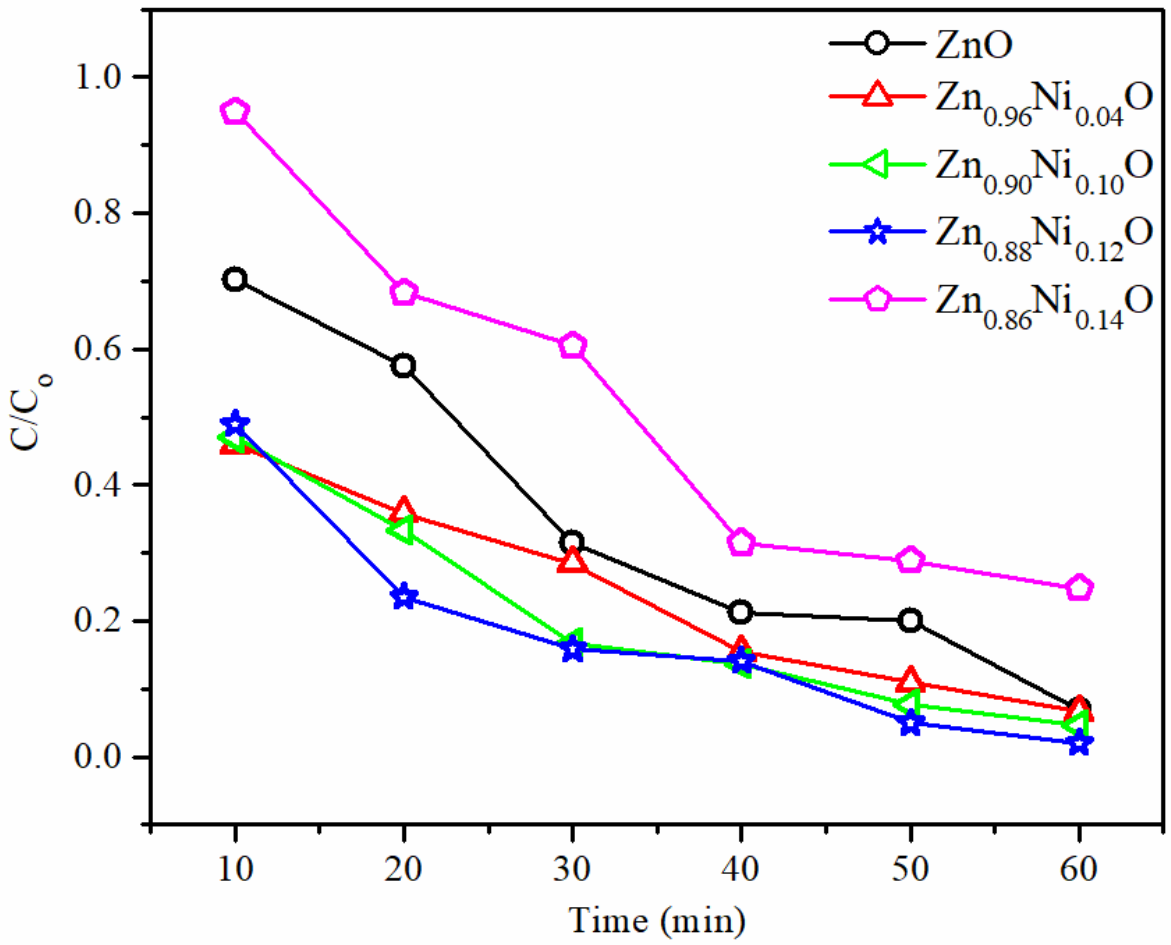

Figure 9

Time resolved concentration profiles for degradation process of MB MB onto ZnO (black), $Zn_{0.96}Ni_{0.04}O$ (red), $Zn_{0.90}Ni_{0.10}O$ (green), $Zn_{0.88}Ni_{0.12}O$ (blue) and $Zn_{0.86}Ni_{0.14}O$ (magenta) nano photocatalysts.

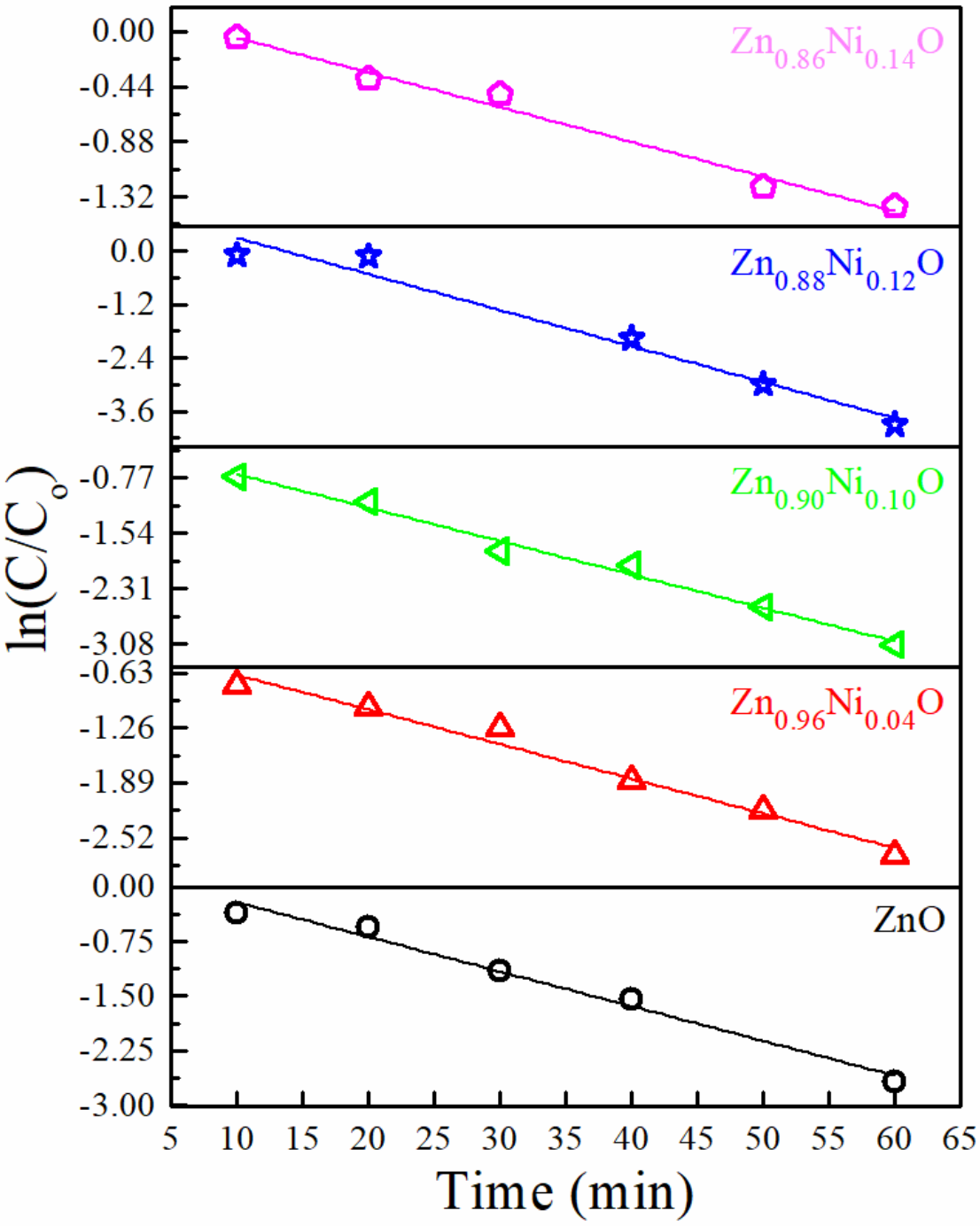

Figure 10

Plots of $\ln(C/C_o)$ vs. time for degradation process of MB onto ZnO (black), $Zn_{0.96}Ni_{0.04}O$ (red), $Zn_{0.90}Ni_{0.10}O$ (green), $Zn_{0.88}Ni_{0.12}O$ (blue) and $Zn_{0.86}Ni_{0.14}O$ (magenta) nano photocatalysts.

Supplementary Files

This is a list of supplementary files associated with this preprint. Click to download.

- Graphicalabstract.png
- Scheme1.png